Dynamics Study of the OH + O_2 Branching Atmospheric Reaction. 4. Influence of Vibrational Relaxation in Collisions Involving Highly Excited Species

J. D. Garrido,† P. J. S. B. Caridade, and A. J. C. Varandas*

Departamento de Química, Universidade de Coimbra, P-3049 Coimbra, Portugal

Received: February 1, 2002; In Final Form: March 13, 2002

The vibrational relaxation processes occurring during collisions of vibrationally excited O_2 and OH are investigated using the quasiclassical trajectory method and a realistic double many-body expansion (DMBE I) potential energy surface for ground-state HO_3. A salient feature is the observation of multiquanta deactivation processes for such high internal energies. It is also shown that the vibrational relaxation of colliding molecules is far less important than the reactive processes leading to formation of "odd-oxygen" (and hence ozone) under stratospheric local thermodynamic disequilibrium conditions.

1. Introduction

The existence of vibrationally hot species[1−10] under conditions of nonlocal thermodynamic equilibrium (or simply local thermodynamic disequilibrium,[10] LTD) in the stratosphere allows the occurrence of endoergic reactions which would not be viable otherwise. Despite this, atmospheric models continue, to our knowledge, to consider only reactions under equilibration conditions. In fact, most attempts to explain the discrepancy between the upper atmospheric model predictions of ozone concentration and satellite observations, known as the "ozone deficit problem",[11−14] have employed equilibrium concentrations of different atmospheric constituents and/or equilibrium rate constants.[15−21] The poor success of such models in resolving the above-mentioned "ozone deficit" leads to the necessity of introducing new ozone sources based on vibrationally excited molecules.[5,10,22−24] Following this idea, other sources of ozone, considering LTD conditions, have been suggested. For example, Wodtke and co-workers[5,25−28] proposed an ozone source with basis on the reaction of vibrationally excited $O_2(v'' \geq 26)$ with ground state O_2, hereafter referred to as the "Wodtke mechanism"

$$O_3 + h\nu(\lambda < 243\ \text{nm}) \rightarrow O_2(X\,^3\Sigma_g^-, v'' \leq 28) + O(^3P) \quad (1)$$

$$O_2(X\,^3\Sigma_g^-, v'' \geq 26) + O_2 \rightarrow O_3 + O(^3P) \quad (2)$$

$$2 \times \{O(^3P) + O_2 + M \rightarrow O_3 + M\} \quad (3)$$

$$\text{NET: } 3O_2 + h\nu(\lambda < 243\ \text{nm}) \rightarrow 2O_3 \quad (4)$$

More recently, we have suggested that ozone could be produced through the reaction[29−31]

$$OH(v', j') + O_2(v'', j'') \rightarrow O_3 + H \quad (5)$$

in conjunction with the three-body recombination of the atomic oxygen produced by other channels of the branching reaction 5, namely

$$OH(v', j') + O_2(v'', j'') \rightarrow HO_2 + O \quad (6)$$

$$\rightarrow O + H + O_2 \quad (7)$$

$$\rightarrow O + O + OH \quad (8)$$

Moreover, further atmospheric ozone sources have been suggested in our Group involving vibrationally excited $O_2(v', j')$[6,7,8] or $HO_2(\boldsymbol{v})$[32] instead of $OH(v')$ in eq 5 [and, correspondingly, in eq 6 to eq 8]; $\boldsymbol{v}$ stands for the three vibrational normal modes of HO_2. In addition, it has been shown that the traditional O_x and HO_x ozone depletion cycles could be reformulated to act as ozone sources.[10,24] Such reformulated cycles could indeed also help to explain[10,24] the so-called "OH surplus" (ref 15, and references therein) in the stratosphere and lower mesosphere predicted by traditional atmospheric chemistry.

In relation to the Wodtke mechanism, several theoretical investigations[6,33,34] have demonstrated that the reactive channel (2) makes a negligible contribution to the destruction of vibrationally excited O_2 at stratospheric temperatures, whereas calculations using quantum reduced-dimensionality methods,[35,36] semiclassical wave packet approaches[37] and quasi-classical trajectories (QCT)[38] have suggested that the experimentally observed jump in the vibrational population of O_2 could partially be due to an enhancement in the vibrational relaxation rates when the system samples regions close to the reaction transition state. However, these studies cannot reproduce the measured sharp increase in the relaxation rate coefficient involving $O_2(v'' = 28)$. Although it has been suggested[10,24] by comparison with available experimental quenching vibrational rates[1,5,25−28,39−45] that reaction should dominate over inelastic processes, it is valuable to confirm such a suggestion by comparing reactive and nonreactive rate constants employing the same potential energy surface and level of theory. This is the major goal of the present work.

Of relevance to this work are the available experimental measurements on the vibrational relaxation of excited OH by collisions with O_2,[1,39−45] but we are unware of similar work devoted to quenching studies of vibrationally excited O_2 molecules and OH radicals when both species are vibrotationally excited.

* To whom correspondence should be addressed. E-mail: varandas@qtvs1.qui.uc.pt.

† Permanent address: Departamento de Física General y Matemática, Instituto Superior de Ciencias y Tecnología Nucleares, 6163 La Havana, Cuba.

10.1021/jp0203245 CCC: $22.00
Published on Web 04/17/2002

As for the methodology, we will employ the well-established QCT method to study the dynamics of the collisional processes

$$OH(v_i', j_i' = 1) + O_2(v_i'', j_i'' = 1) \rightarrow OH(v_f', j_f') + O_2(v_f'', j_f'') \quad (9)$$

by considering various combinations of initial vibrational quantum numbers v_i' and v_i''. Although an exact solution would involve a quantum dynamics treatment, this is essentially out of the question, given the dimensionality of the problem and the number of open channels involved. The alternatives are therefore approximate quantum or semiclassical treatments, and the QCT method which is exact within the context of classical mechanics (for a review focusing on four-atom atmospheric reactions, see ref 8). Following previous work,[29−31] we have adopted the latter approach in the present work because it can afford an exact treatment within the full dimensionality of the problem. Similarly, the realistic single-valued double many-body expansion (DMBE I[46]) potential energy surface for the electronic ground state of HO_3 will be employed. Although, an improved version of this surface is available,[47] we insist on using DMBE I to make the comparison with our previous reactive studies[29−,31] even more realistic. Note also that both OH and O_2 reactant molecules are initially kept on their rotational ground states. Although a kinetics treatment would involve an average over all initial rotational states, such a mammoth task is probably unjustified on the basis of previous work.[29,30,52] Thus, we omit heretofore the specification of the initial rotational state.

The paper is organized as follows. Section 2 provides a brief survey of the computational method. The results of calculations for deactivation processes are presented and discussed in section 3, whereas section 4 presents an analysis about the influence of deactivation processes over chemical reactions. Section 5 gathers the major conclusions.

2. Computational Details

Following previous papers of this series,[29−31] we have employed the QCT method as implemented in the MERCURY/VENUS96[48] codes, suitably adapted to study the title collisional processes. Calculations have been carried out for diatom−diatom translation energies over the range $0.5 \leq E_{tr}/\text{kcal mol}^{-1} \leq 10$, as summarized in Table 1. Although lower energies play an important role in the determination of thermal rate coefficients at low temperatures, they are computationally too heavy for practical purposes. However, this problem can be overcome if a realistic model is used to extrapolate the cross section to lower translational energies (i.e., to represent the excitation function). As it will be shown later, this is hopefully the case. The initial diatomic−diatomic separation has been fixed at 9 Å to make the interaction essentially negligible. The optimum step size for numerical integration of the equations of motion has been determined according to the usual procedures. To select the maximum value of the impact parameter (b_{max}) which leads to vibrational relaxation we have run batches of 100 trajectories for fixed values of b until the standard deviation between the vibrational energy of the product in the nonreactive trajectories and the initial vibrational energy of corresponding molecule reaches a value similar to the error in the conservation of the total energy. The calculated values are reported in Table 1. Batches of 2000 trajectories have then been carried out for each translational energy (E_{tr}) and vibrational−rotational combination making a total of 4×10^5 trajectories.

The energetics of the involved processes is best seen in the diagram of Figure 1, where the line segments on the reactants

TABLE 1: Summary of the Trajectory Calculations for the $OH(v_i') + O_2(v_i'') \rightarrow OH(v_f') + O_2(v_f'')$

v'	v''	$E_{vib/rot}$ kcal mol^{-1}	E_{tr} kcal mol^{-1}	b_{max} Å	$\sigma^{OH} \pm \Delta\sigma^{OH}$ Å^2	$\sigma^{O_2} \pm \Delta\sigma^{O_2}$ Å^2
9	13	135.3515	0.5	6.2	46.25 ± 1.3	38.10 ± 1.3
			1.0	6.0	34.55 ± 1.1	27.31 ± 1.1
			2.5	5.8	24.94 ± 1.0	20.98 ± 0.9
			5.0	5.7	21.84 ± 0.9	16.18 ± 0.8
			10.0	5.6	19.11 ± 0.8	15.52 ± 0.9
9	16	145.8698	0.5	6.3	34.98 ± 1.3	35.47 ± 1.3
			1.0	6.0	29.86 ± 1.1	29.12 ± 1.1
			2.5	5.8	24.68 ± 1.0	23.51 ± 1.0
			5.0	5.7	20.31 ± 0.9	18.58 ± 0.9
			10.0	5.6	16.90 ± 0.8	18.03 ± 0.9
6	27	157.3528	0.5	6.4	23.16 ± 1.1	32.62 ± 1.3
			1.0	6.0	18.95 ± 0.9	27.95 ± 1.1
			2.5	5.8	18.39 ± 0.9	26.37 ± 1.0
			5.0	5.8	16.38 ± 0.9	25.62 ± 1.0
			10.0	5.8	15.17 ± 0.8	21.98 ± 1.0
9	27	177.7281	0.5	6.6	11.97 ± 0.8	12.52 ± 0.9
			1.0	6.2	10.57 ± 0.8	11.47 ± 0.8
			2.5	6.0	10.63 ± 0.7	11.82 ± 0.8
			5.0	5.8	10.41 ± 0.7	11.94 ± 0.7
			10.0	5.8	11.52 ± 0.7	12.10 ± 0.8

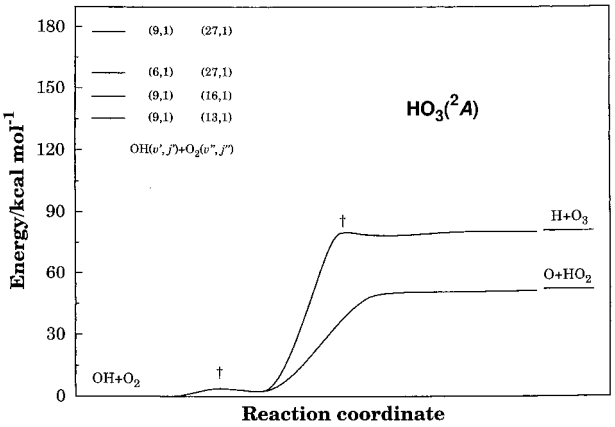

Figure 1. Schematic diagram showing the energetics of the different collisional processes studied in the present work according to the HO_3 DMBE I potential energy surface. The daggers indicate the saddle points for the reactions $H + O_3 \rightarrow HO_3 \rightarrow OH + O_2$ and $O + HO_2 \rightarrow HO_3 \rightarrow OH + O_2$.

side indicate the various vibrational combinations (as estimated from the HO_3 DMBE I potential energy surface[46]) employed in the present work. Note that the combination $OH(v' = 0) + O_2(v'' = 16)$ (see ref 29) corresponds roughly to the "effective" threshold energy (the true threshold energy occurs for $v'' \approx 13$) for HO_2 formation. It lies approximately 66 kcal mol^{-1} above the zero-point energy of the reactants channel (see ref 30) and 14 kcal mol^{-1} over the $HO_2 + O$ products. However, the bold part of the reactive processes (eq 5 to eq 8) occurs roughly at total energies of 128 kcal mol^{-1}, and hence we focused in this work on such energy regimes.

The boxing procedure used to assign the final vibrational energy E_f^x for each molecule (x may be OH or O_2) in the products, defines the final quantum state $E_f^x(v)$ and associated spread of energy for the v level as

$$\frac{E^x(v) + E^x(v-1)}{2} < E_f^x(v) < \frac{E^x(v+1) + E^x(v)}{2} \quad (10)$$

where, in an obvious notation, $E^x(v)$ is the energy of v-th vibrational state of molecule x. Note that we have artificially defined the $v = -1$ as lying halfway between the minimum of the potential energy curve and the $v = 0$ level. Thus, it

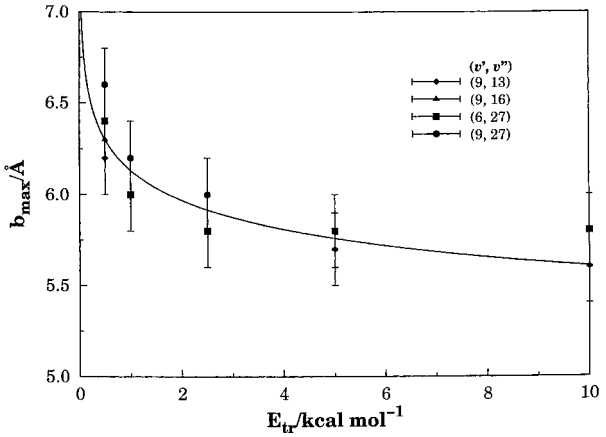

Figure 2. Energy dependence of the maximum impact parameter for some vibrotational combinations.

somewhat more restrictive than the purely classical approach which consists of identifying the $v = -1$ level with the bottom of the potential energy curve ($v = -1/2$). In any case, given the magnitude of the vibrational excitations involved in the title processes, such an arbitrariness (for papers which address the dificulties encoutered in the related problem due to zero-point energy leakage, see refs 8 and 49 and references therein) discussion should play no role in the analysis of the products. Thus, trajectories will be considered as vibrationally elastic if the following relation is satisfied

$$\frac{E^x(v_i - 1) - E^x(v_i)}{2} < E_f^x(v) - E^x(v_i) < \frac{E^x(v_i + 1) - E^x(v_i)}{2} \tag{11}$$

A final remark to note that the traditional boxing procedure that we are employing is subject to significant error if the number of populated bins is small.[50] We emphasize though that this is not the case in the present work because the excitation energies involved are quite high.

3. Results and Discussion

Table 1 summarizes the trajectory calculations carried out in the present work for the relaxation process (9) when both molecules are vibrationally excited and the internal energy is sufficiently high to open the reactive channels. Note that in previous papers,[29−31] the maximum impact parameter has been shown to increase with internal energy of the reactants for a fixed translational energy. It turns to be now essentially invariant with internal energy, whereas slightly increasing with decreasing translational energy. Such a variation with translational energy is well described by the form

$$b_{max} = \frac{b}{E_{tr}^m} \tag{12}$$

where b and m are disposable parameters, as seen from Figure 2 which shows the dependence of b_{max} on E_{tr} for collisions where both molecules are vibrationally excited. It is seen that eq 12 mimics the general trends of the calculations. Note that we have selected the value appropriate for studying both the relaxation of OH and O_2 as a maximum impact parameter, when they are both on their maximum excitations. It turns out that a separate optimization for individual vibrational combinations corroborates our selection.

Figure 3 shows collison lifetimes of both vibrationally elastic and inelastic processes for the initial vibrational combinations

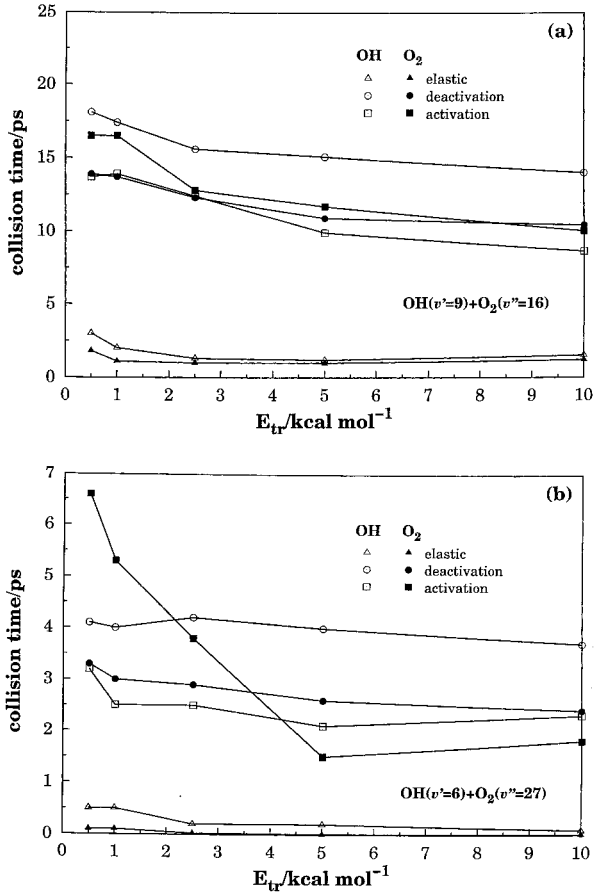

Figure 3. Dependence of the collisional average lifetime on translational energy: (a) OH(9) + O_2(16); (b) OH(6) + O_2(27).

OH(9) + O_2(16) and OH(6) + O_2(27), as calculated using the model reported elsewhere.[29] Note that the solid symbols in this and all subsequent plots refer to O_2, whereas the open symbols are for OH. The results show that the time for elastic collisions is, as it might be anticipated, shorter than for the inelastic ones. This may be rationalized by the fact that an inelastic process has to involve some coupling of the various degrees of freedom, possibly induced by the long range dipole−quadrupole and quadrupole−quadrupole electrostatic interactions (not to mention Coulombic forces of the dispersion type). Note that in both cases, the calculated lifetimes are slowly decreasing functions of the translational energy. Moreover, for all initial conditions, the time for OH deactivation turns out to be longer than for O_2. This result may in turn be explained having in mind that the size of the vibrational and rotational quanta for the hydroxyl radical are larger than for molecular oxygen. Because the deactivation time of one of the partners correlates with the activation time of the other, such a result implies that the activation of O_2 has to be a slow process. The differences in quantum size may also explain why O_2 deactivation times (or, alternatively, OH excitation times) during the OH(6) + O_2(27) collisional process have to be shorter than the OH deactivation (O_2 excitation) times in OH(9) + O_2(16).

The ratios between the final and initial values of relative translational energy and internal energy (for each molecule) as a function of translational energy are displayed in Figure 4. It is seen from panel (a) of Figure 4 that the translational energy ratios drastically diminish with increasing translational energy until they reach a constant value for the asymptotic hard-sphere regime of the cross section (this point will be emphasized later). In turn, panel (b) shows that the efficiency on the deactivation

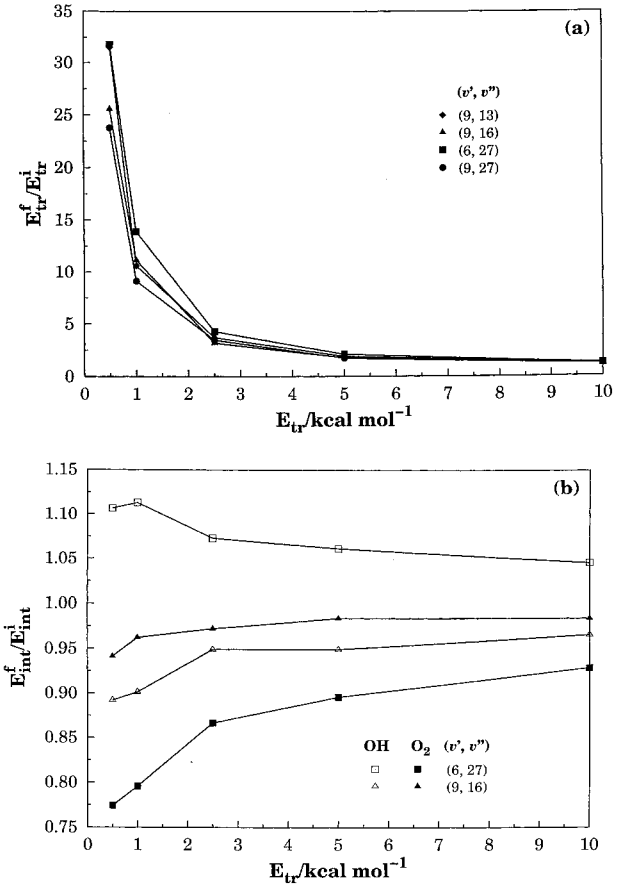

Figure 4. Ratios, for some vibro-rotational combinations, between initial and final average values: (a) translational energy; (b) internal energy.

(or activation if it is the case) decreases with increasing translational energy. For example, the ratios in the upper curve referring to activation of OH decrease from slightly over 1.1 at $E_{tr} = 1$ kcal mol^{-1} to 1.05 at $E_{tr} = 10$ kcal mol^{-1}. Conversely, the bottom curve referring to deactivation of O_2 varies from about 0.8 at $E_{tr} = 1$ kcal mol^{-1} to 0.9 at $E_{tr} = 10$ kcal mol^{-1}.

Figure 5 shows, for OH and O_2, the state-to-state deactivation probabilities for two different combinations of vibrational excitation. The most remarkable feature from this Figure is perhaps the fact that the energy tranfer processes are dominated by multiquanta vibrational transitions, with the probability deactivation being in general larger for less excited molecules. In addition, it is relevant to note that vibrational activation is specially significant for the less excited molecules. For example, a comparison of panels (a) and (b), or (c) and (d), show that the transition probabilities are typically larger by a factor of about 2 for the less excited combination. Because there are many vibrational levels that can be populated both on the activation and deactivation processes, the V−V′ energy transfer collisions are expected to be more relevant than in the case where one of the partners is at or close to the ground vibrational state. To our knowledge, energy transfer processes involving two chemically distinct highly vibrationally excited species have not been studied thus far. We further observe that, despite so many vibrational states at play, only very few near-resonance conditions have been detected. An example is perhaps the combination OH(9) + O_2(16) to yield OH(8) + O_2(17) or OH(8) + O_2(18). The energy mismatch lies in this case between 77 cm^{-1} and 124.7 cm^{-1}. Such a resonance behavior manifests itself in a larger transition probability, as can be observed from panel (b) of Figure 5 for the O_2 transition $v_i'' = 16$ to $v_i'' = 18$. A final comment to note that, for a given value of the final vibrational quantum number, there is a tendency to increase the transition probability with decreasing translational energy specially in the case of less excited molecules. For example, Figure 5(b) shows an increase of a factor of 2−3 in going from $E_{tr} = 10$ kcal mol^{-1} to $E_{tr} = 0.5$ kcal mol^{-1} at $v_f'' = 12$. For more activated molecules, the probability of deactivation is on average essentially constant for all final vibrational quantum numbers. For less excited ones, there is generally a decrease of the transition probability with the number of vibrational quanta transferred.

3.1. Specific Initial-State Deactivation and Activation Cross Sections. The specific initial-state deactivation probability $P^{x,\downarrow}_{E_i}$ (i.e., the probability of transition from the initial vibrational state corresponding to the energy E_i^x for the x species to any smaller final vibro-rotational energy E_f^x of deactivated molecule) can be defined as

$$P^{x\downarrow}_{E_i} = \sum_{E_f^x = E_0^x}^{E^x_{v_i^x - 1}} P^{x\downarrow}_{E_i, E_f^x} \tag{13}$$

where the downarrow has an obvious meaning, $E_i = E_i^{O_2} + E_i^{OH}$ is the total initial internal energy, and the state-to-state deactivation probability is given by

$$P^{x\downarrow}_{E_i, E_f^x} = N^{x\downarrow}_{E_i}/N_{E_i}$$

with

$$N^{x\downarrow}_{E_i} = \sum_{E_f^x = E_0^x}^{E^x_{v_i^x - 1}} N^{x\downarrow}_{E_i, E_f^x}$$

being the total number of trajectories corresponding to vibrational deactivation processes from the initial vibro-rotational state E_i to any smaller final vibro-rotational state E_f^x of the deactivated species x, and N_{E_i} the total number of trajectories run. Note that (although equivalent) we have preferred to use energies rather than vibrational quantum numbers to identify the initial and final states because the model excitation function to be presented later in eq 17 is defined in terms of the internal energy. Thus, the specific initial-state cross section assumes the form

$$\sigma^{x\downarrow}_{E_i}(E_{tr}) = \pi b^2_{max}(E_{tr}) P^{x\downarrow}_{E_i}(E_{tr}) \tag{14}$$

with the associated 68% uncertainaties being given by

$$\Delta\sigma^{x\downarrow}_{E_i} = \left(\frac{N_{E_i} - N^{x\downarrow}_{E_i}}{N_{E_i} N^{x\downarrow}_{E_i}} \right)^{1/2} \sigma^{x\downarrow}_{E_i} \tag{15}$$

Similarly, the initial-state activation probabilities assume the form

$$P^{x\downarrow}_{E_i} = \sum_{E_f = E^x_{v_i^x + 1}} P^{x,\downarrow}_{E_i, E_f} \tag{16}$$

with expressions corresponding to the above ones (for the deactivation cross section) being applicable to the initial-state activation cross section. Note that the range of translational energies is too short for the V−T mechanism to play any significant role, and hence the activation cross sections are mostly due to V−V′ and V−R mechanisms.

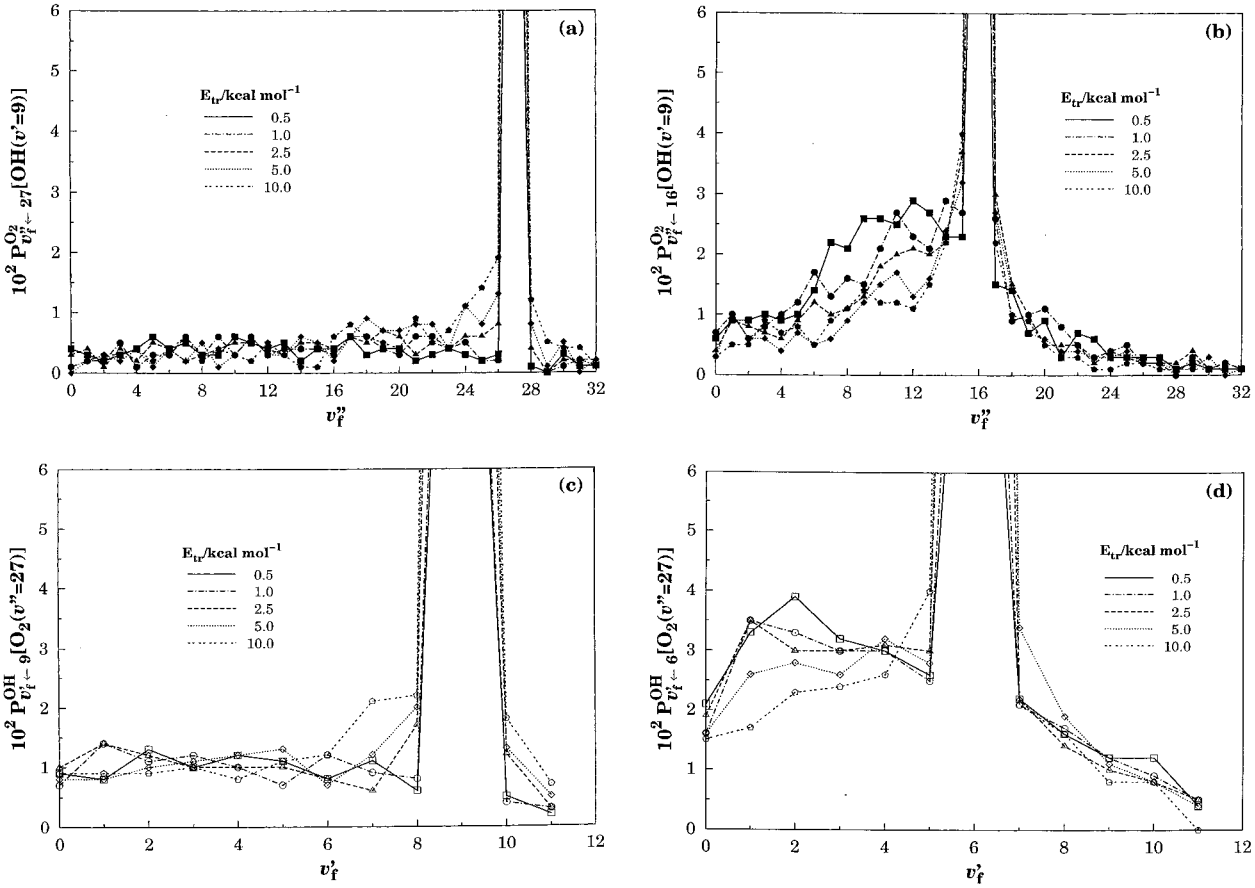

Figure 5. State-to-state transition probabilities as a function of translational energy: (a) OH(9) + O_2(16) for O_2 relaxation; (b) OH(9) + O_2(16) for O_2 relaxation; (c) OH(6) + O_2(27) for OH relaxation; and (d) OH(9) + O_2(27) for OH relaxation.

We now examine the shape of the specific initial-state deactivation and activation cross sections vs translational energy (excitation functions), which are illustrated in Figure 6 together with the associated 68% error bars. Note that panels (a) and (b) refer to the deactivation, whereas (c) and (d) are for the activation process. We should also note that the values of the specific initial-state deactivation cross sections reported in the present work for the highly vibrationally excited molecules are much smaller than those calculated[51] when the total internal energy is below 128 kcal mol^{-1} (this corresponds approximately to the threshold energy for reaction) as a result of the competition between the reactive (with a very high effective cross section[29−31]) and nonreactive collisional processes. It is interesting to observe that such a cross section for O_2 deactivation in the process OH(9) + O_2(27) is quite similar to the corresponding OH deactivation cross section. This may be justified on the basis that the energy content of both molecules is very similar, having in perspective the difference in the well depths of both molecules. Although a reasonably similar behavior is found for OH(9) + O_2(16), no such trend applies to the other combinations. For these, the general pattern is that the more (less) vibrationally excited species tends to deactivate (activate) more. We further observe that, in general, all mechanisms (V−T, V−R, and V−V′) are expected to contribute to a given transition process. However, in the case of the present work, the V−T mechanism is found to dominate for the deactivation processes which may be rationalized as a consequence of the observed energy mismach. In fact, the relative weights of the V−V′ and V−R mechanisms on the deactivation process are found to change with translational and internal energy from a few percent (for high internal energies and low translational energies) up to more than 30% (for the opposite energetic regimes).

To analytically describe the dependence of the specific initial-state cross sections with the translational energy, we have adopted the form

$$\sigma^{x}_{E_i} = \frac{\left(\sum_{k=0}^{3} c_k^x E_i^k\right)\exp(-m_1^x E_i)}{E_{\mathrm{tr}}^{\mathrm{n}}} + \left(\sum_{k=0}^{3} d_k^x E_i^k\right)\exp(-m_2^x E_i) \quad (17)$$

Figure 6 shows the fitted function together with the calculated points and associated error bars. The value of the parameter $n = 0.434\,16$ has been constrained to be the same for all reactive and nonreactive processes and all internal energies. It has been determined from a least-squares fitting procedure following the approach used elsewhere.[52,31] The remaining coefficients in eq 17 have been determined from a least-squares fit to the data referring to a specific molecule; the optimum numerical values of all fitting parameters are reported in Table 2. Clearly, the model provides a satisfactory fit of the calculated data.

Because the interaction time decreases with increasing translational energy, the deactivation cross section curves in Figure 6 show a negative slop over the range of studied translational energies with a tendency to flatten after 2.5 kcal mol^{-1} or so. This is due to the decrease in interaction time which prevents energy transfer, and hence leads to a kind of hard-spheres behavior at those high collisional energies. Note that, for such energy regimes, the coupling between the vibrational modes of both molecules promoted by long range interactions

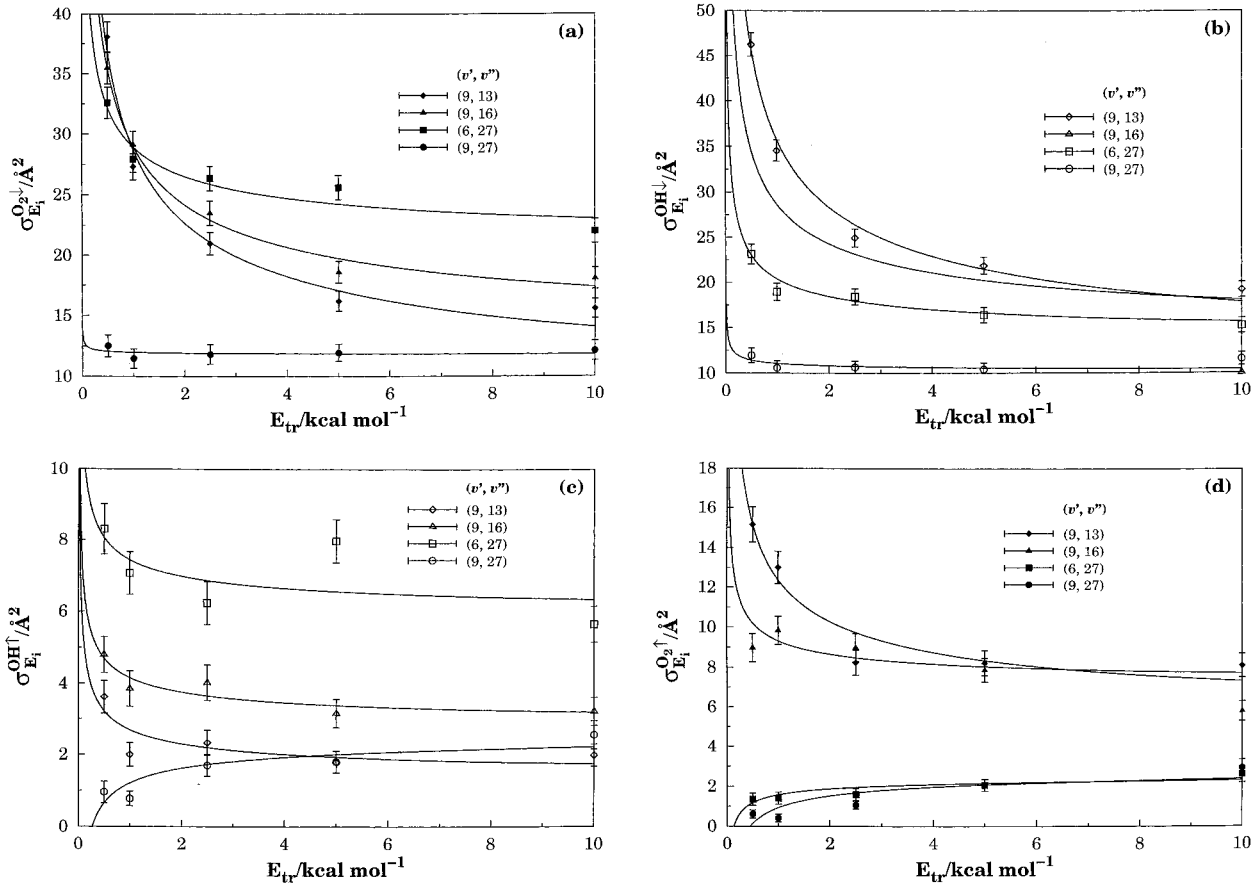

Figure 6. Specific cross section σ^x as a function of the translational energy: (a) deactivation of O_2; (b) deactivation of OH; (c) activation of OH; and (d) activation of O_2. Also indicated are the 68% error bars and the model in eq 17.

TABLE 2: Numerical Values of the Coefficients in eq 17

process	a_0	a_1	a_2	a_3	m_1
$O_2^{\downarrow}$	−20 276.7	398.816	−2.560 03	0.005 390 82	0.014 745 1
$O^{\downarrow}_{2,v''<13}$	−33 860.4	648.017	−4.087 06	0.008 519 63	0.014 745 1
$O_2^{\uparrow}$	−1357.37	38.993	−0.317 353	0.000 787 42	0.014 745 1
$OH^{\downarrow}$	−2236.43	58.9508	−0.450 487	0.001 068 26	0.011 696 2
$OH^{\downarrow}_{v''<4}$	5916.29	−110.512	0.698 64	−0.001 483 73	0.011 696 2
$OH^{\uparrow}$	3650.88	−74.6071	0.507 324	−0.001 145 13	0.011 696 2
process	b_0	b_1	b_2	b_3	m_2
$O_2^{\downarrow}$	206 865	−4153.87	27.5681	−0.060 306 3	0.024 098 2
$O^{\downarrow}_{2,v''<13}$	87 639.4	−1707.4	11.0448	−0.023 670 3	0.024 098 2
$O_2^{\uparrow}$	−120 789	2355.94	−15.2209	0.032 613 5	0.024 098 2
$OH^{\downarrow}$	32 097.4	−861.731	6.616 26	−0.014 337 6	0.037 185 2
$OH^{\downarrow}_{v''<4}$	814 630	−16094.4	105.197	−0.227 05	0.037 185 2
$OH^{\uparrow}$	607 008	−12105.3	79.7959	−0.173 501	0.037 185 2

leads preferentially to chemical reaction rather than vibrational relaxation. We will return to this point later.

3.2. Specific Deactivation Rate Coefficients. From the specific initial-state deactivation cross sections and assuming a Maxwell−Boltzmann distribution over the translational energy, the specific thermal deactivation rate coefficients are obtained as

$$k^{x\downarrow}(E_i, T) = g_e(T)\left(\frac{2}{k_B T}\right)^{3/2}\left(\frac{1}{\pi\mu}\right)^{1/2}\int E_{tr}\sigma^x_{E_i}\exp\left(-\frac{E_{tr}}{k_B T}\right)dE_{tr} \quad (18)$$

where $g_e(T) = 1/3[1 + \exp(-205/T)]^{-1}$ is the appropriate electronic degeneracy factor, k_B is the Boltzmann constant, μ is the reduced mass of the colliding diatomic molecules, and T is the temperature in Kelvin. Integration of eq 18 leads to

$$k^{x\downarrow}(E_i, T) = g_e(T)\left(\frac{8}{\pi\mu}\right)^{1/2}(k_B T)^{1/2-n} \times [\Gamma(2-n)f^x(E_i)\exp(-m_1^x E_i) + g^x(E_i)\exp(-m_2^x E_i)(k_B T)^n] \quad (19)$$

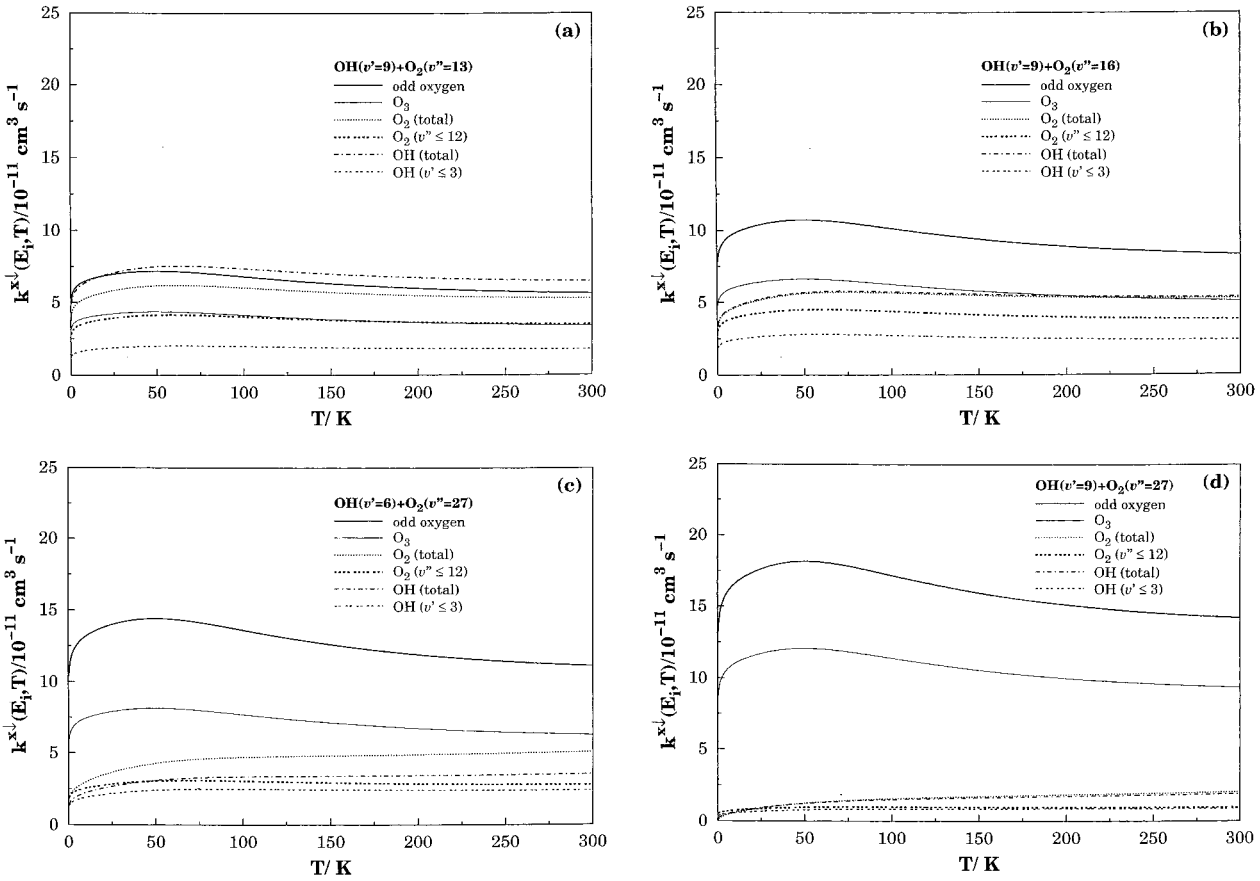

Figure 7. Specific thermal deactivation rate coefficients: (a) OH(9) + O_2(13); (b) OH(9) + O_2(16); (c) OH(6) + O_2(27); and (d) OH(9) + O_2(27).

where

$$f^x(E_i) = \sum_{k=0}^{3} c_k^x E_i^k \tag{20}$$

and

$$g^x(E_i) = \sum_{k=0}^{3} d_k^x E_i^k \tag{21}$$

Figure 7 shows the calculated specific rate coefficients as a function of temperature. Note that the specific deactivation rate coefficients vanish as $T \rightarrow 0$, as implied from eq 19. We further observe that they should be viewed with caution at such ultralow temperatures, particularly having in mind that the cross section has been extrapolated to low translational energies. Also shown in Figure 7 are the specific rate coefficients for vibrational deactivation up to the level $v' = 3$ of OH and $v'' = 12$ of O_2, which correspond to the first vibrational combination capable of leading to reaction and, hence, to ozone production [i.e., OH(9) + O_2(13) or OH(3) + O_2(27) can produce ozone]. Because as noted above, the differences in specific deactivation cross section (for any final vibrational quantum number) for OH and O_2 in the combinations OH(9) + O_2(27) and OH(9) + O_2(16) are small, it is reasonable to expect that the specific thermal deactivation rate coefficients have similar values for both molecules at such initial combinations, as indeed observed from panels (b) and (d) of Figure 7. In turn, panels (a) and (c) show that the specific deactivation rate coefficients of O_2 and OH for other initial vibrational combinations have significant differences. However, a more interesting comparison will involve the specific thermal reactive rate coefficients and the nonreactive ones. This can be appreciated by comparing, for all panels but (a), the curves in solid with those in dashed. Note that the thin solid line corresponds to direct ozone formation, while that in bold corresponds to total odd oxygen production. We further note that the differences between the reactive and nonreactive rate coefficients increase with internal energy reaching a 5-fold magnitude at $T = 300$ K. Indeed, an 11-fold factor can even be observed if the compariosn is done with the deactivation process up to level $v'' = 12$ for the combination OH(9) + O_2(27).

Figure 8a shows the vibrationally averaged thermal deactivation rate for all final vibrational states

$$k^{\downarrow}(T) = \frac{\sum_{E_i^{OH}=E_{i0}^{OH}} \sum_{E_i^{O_2}=E_{i0}^{O_2}} \omega_{E_i}^{OH} \omega_{E_i}^{O_2} k^{O_2\downarrow}(E_i^{OH} + E_i^{O_2} \geq 130, T)}{\sum_{E_i^{OH}=E_{i0}^{OH}} \sum_{E_i^{O_2}=E_{i0}^{O_2}} \omega_{E_i}^{OH} \omega_{E_i}^{O_2}} \tag{22}$$

We also show the corresponding vibrational averaged rate coefficients for final vibrational quantum numbers $v_f'' < 13$

$$k^{\downarrow,v_f''<13}(T) = \frac{\sum_{E_i^{OH}=E_{i0}^{OH}} \sum_{E_i^{O_2}=E_{i0}^{O_2}} \omega_{E_i}^{OH} \omega_{E_i}^{O_2} k^{O_2\downarrow,v_f''<13}(E_i^{OH} + E_i^{O_2} \geq 130, T)}{\sum_{E_i^{OH}=E_{i0}^{OH}} \sum_{E_i^{O_2}=E_{i0}^{O_2}} \omega_{E_i}^{OH} \omega_{E_i}^{O_2}} \tag{23}$$

In both cases, the populations $\omega_{E_i}^{OH}$ and $\omega_{E_i}^{O_2}$ have been taken from refs 2 and 5. Moreover, we give for comparison the total

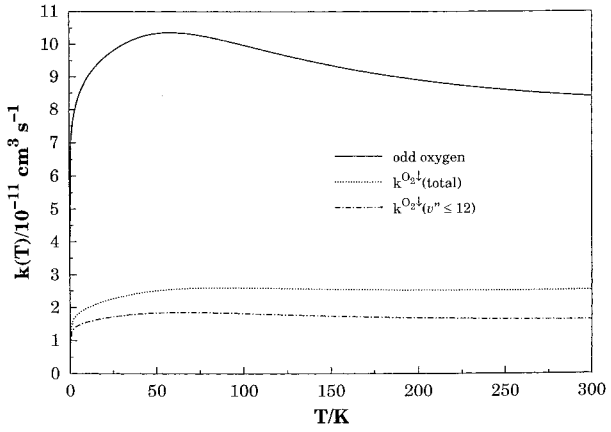

Figure 8. Vibrational average thermal deactivation rate constant.

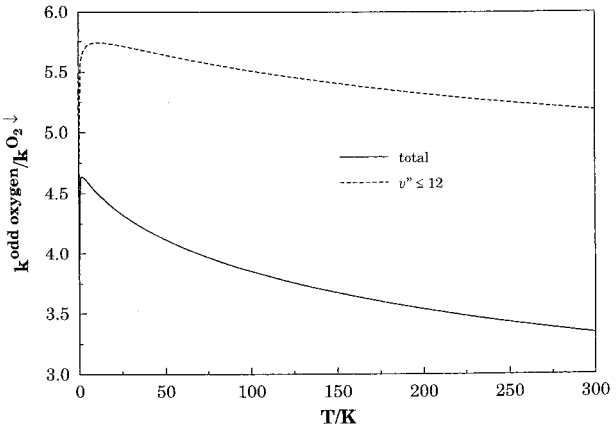

Figure 9. Ratio of vibrationally averaged thermal rate coefficients for formation of "odd-oxygen" and vibrational deactivation.

vibrationally averaged thermal rate coefficient for reaction $k^{\text{total}}(T)$ reported elsewhere.[31] As Figure 9 shows, the ratios $k^{\text{total}}(T)/k^{\downarrow}(T)$ and $k^{\text{total}}(T)/k^{\downarrow,v''_f<13}(T)$ are larger than 3 or 5, depending on the criterion adopted to define the nonreactive thermal rate coefficients. The more restrictive criterion (i.e., which leads-to-smaller ratios) case counts as nonreactive any deactivation process, including those final states whose internal energy lies above 128 kcal mol^{-1} and hence are still capable of leading to reaction. The less restrictive one counts as nonreactive the final states only those lying below the above threshold energy. For a typical temperature of $T = 150$ K, such ratios amount to 3.7 and 5.4.

4. Influence of Vibrational Deactivation on Chemical Reaction

Considering reactions 5−8 and 9, the temporal variation of $O_2(v'')$ concentration (represented as $[O_2(v'')]$) can be expressed as

$$\frac{d[O_2(v'')]}{dt} = \sum_{v'} \Phi_{v''}(v') + s_{v''} - \sum_{v'} k^{\text{total}}_{v'',v'}[O_2(v'')][OH(v')] \tag{24}$$

where $k^{\text{total}}_{v'',v'}$ is the specific thermal rate coefficient for formation of "odd-oxygen", $s_{v''}$ represents any source of vibrationally excited oxygen in the level v'', and $\Phi_{v''}(v')$ is the net flux of molecules entering level v'' defined as

$$\Phi_{v''}(v') = \left\{ \sum_{\tilde{v}''=v''+1} k^{\downarrow}_{\tilde{v}'',v''}(v')[O_2(\tilde{v}'')] - \sum_{\tilde{v}''=v''+1} k^{\downarrow}_{\tilde{v}'',\tilde{v}''}(v')[O_2(v'')] + \sum_{\tilde{v}''=0}^{v''-1} k^{\uparrow}_{\tilde{v}'',v''}(v')[O_2(\tilde{v}'')] - \sum_{\tilde{v}''=0}^{v''-1} k^{\uparrow}_{\tilde{v}'',\tilde{v}''}(v')[O_2(v'')] \right\} [OH(v')] \tag{25}$$

Because the reactions leading to "odd-oxygen" occur effectively for $v'' > 12$, one gets

$$\frac{d\sum_{v''=13}[O_2(v'')]}{dt} = -\sum_{v'=0}\sum_{v''=13} k^{\downarrow}_{v'',v'}[O_2(v'')][OH(v')] - \sum_{v'=0}\sum_{v''=13} k^{\text{total}}_{v'',v'}[O_2(v'')][OH(v')] + \sum_{v''=13} s_{v''} \tag{26}$$

$$= -(k^{\downarrow,v''_f<13}(T) + k^{\text{total}}(T))[O_2][OH] + \sum_{v''=13} s_{v''} \tag{27}$$

where $[O_2]$ and $[OH]$ represent the total concentrations of excited molecules over the relevant range of vibrational quantum numbers for each species. Clearly, the thermal rate coefficient $k^{\text{total}}(T)$ largely overpasses the corresponding vibrational deactivation coefficients. Thus, eq 27 leads to the conclusion that vibrational deactivation by collisions with OH radicals cannot quench the population of vibrationally excited molecules before chemical reaction takes place leading to formation of "odd-oxygen". Of course, our reasoning is based on the LTD assumption in the upper atmosphere. Considering that the improved HO_3 DMBE II potential energy surface[47] predicts an increasing reactivity,[52] we can expect a further decrease of the deactivation thermal rate coefficients and, hence, a reinforcement of the previous statement.

The overall influence of the mechanism discussed in the present work on ozone formation in the upper atmosphere obviously requires the analysis of other factors.[10,24] For example, because there is a flux of molecules between the nonreactive and reactive levels, the existence of other vibrationally excited molecules may enhance chemical reactivity through V−V′ activation processes, in particular by collisions of O_2 with vibrationally excited N_2 and subsequently through collisions of those medium-excited O_2 molecules with each other (which promotes self-deactivation of one and self-activation of the other). Another crucial point to discuss is the real separation of the vibrational population from the Boltzmann distribution in the stratosphere. Of course, all such issues are outside the scope of the present work (ref 53, and papers therein).

5. Conclusions

We have carried out a QCT study of vibrational relaxation of O_2 and OH when both molecules are in high vibrationally excited states. The selected initial internal energies lead to the vibrational relaxation under energetic conditions which competes with chemical reaction. Single-quantum transitions have been found in the present work to have probabilities similar to multiquanta ones, with this mechanism playing in fact the major role in the deactivation process. It has also been found that the calculated specific initial-state deactivation cross sections,

thermal specific deactivation rate coefficients and vibrationally averaged thermal deactivation rate coefficients for the internal energies used in the present calculations are significantly smaller than the corresponding kinetic parameters for internal energies bellow 128 kcal mol^{-1} (which will be reported in a separate publication[51]) and the reactive rate coefficients for "odd-oxygen" formation. More quantitatively, the total vibrationally averaged thermal rate coefficient for "odd-oxygen" formation is between 3 and 5 times larger than the corresponding rate coefficient for vibrational deactivation over the studied range of temperatures. Not surprisingly, comparison with experimental data for such vibrational relaxation processes cannot be done due to the unavailability of such data. The present results stress the importance of taking into consideration both reactive and inelastic processes in any realistic assessment of the stratospheric ozone chemistry. Furthermore, they corroborate a recent suggestion[10,24] that, under LTD conditions, the HO_3 system may play an important role in ozone formation.

Acknowledgment. This work has the support of Fundação para a Ciência e Tecnologia, Portugal. Financial assistance to one of us (J.D.G.) by the German Academic Exchange Service (DAAD) and the Third World Academy of Sciences (TWAS Research Grant No. 97-144, RG/CHE/LA) is also appreciated.

References and Notes

(1) Finlayson-Pitts, B. J.; Kleindienst, T. E.; Ezell, M. J.; Toohey, D. W. *J. Chem. Phys.* **1981**, *74*, 4533.
(2) Ohoyama, H.; Kasai, T.; Yoshimura, Y.; Kuwata, H. *Chem. Phys. Lett.* **1985**, *118*, 263.
(3) Steinfeld, J. I.; Adler-Golden, S. M.; Gallagher, J. W. *J. Phys. Chem. Ref. Data* **1987**, *16*, 911.
(4) Klenerman, D.; Smith, I. W. M. *J. Chem. Soc., Faraday Trans. 2* **1987**, *83*, 229.
(5) Miller, R. L.; Suits, A. G.; Houston, P. L.; Toumi, R.; Mack, J. A.; Wodtke, A. M. *Science* **1994**, *265*, 1831.
(6) Varandas, A. J. C.; Wang, W. *Chem. Phys.* **1997**, *215*, 167.
(7) Wang, W.; González-Jonte, R.; Varandas, A. J. C. *J. Phys. Chem.* **1998**, *102*, 6935.
(8) Varandas, A. J. C. *Int. Rev. Phys. Chem.* **2000**, *19*, 199.
(9) Geiser, J.; Dylewski, S. M.; Mueller, J. A.; Willson, R. J.; Toumi, R.; Houston, P. L. *J. Chem. Phys.* **2000**, *112*, 1279.
(10) Varandas, A. J. C. *ChemPhysChem* **2002**, *3*, 101.
(11) Froidevaux, L.; Allen, M.; Yung, L. Y. *J. Geophys. Res.* **1985**, *90*, 12999.
(12) Natarajan, M.; Callis, L. B.; Boughner, R. E.; Russell III, J. M.; Lambeth, J. D. *J. Geophys. Res.* **1986**, *91*, 1153.
(13) Callis, L. B. M.; Natarajan, M.; Boughner, R. E.; Russell , J. M., III; Lambeth, J. D. *J. Geophys. Res.* **1986**, *91*, 1167.
(14) Jackman, C. H.; Stolarski, R. S.; Kaye, J. A. *J. Geophys. Res.* **1986**, *91*, 1103.
(15) Summers, M. E.; Conway, R. R.; Siskind, D. E.; Stevens, M. H.; Offermann, D.; Riese, M.; Preusse, P.; Strobel, D. F.; Russell, J. M., III. *Science* **1997**, *277*, 1967.
(16) Crutzen, P. *Science* **1997**, *277*, 1951.
(17) Natarajan, M.; Callis, L. B. M. *Geophys. Res. Lett.* **1989**, *16*, 473.
(18) Eluszkiewicz, M. A. J.; Allen, M. *J. Geophys. Res.* **1993**, *98*, 1069.
(19) Siskind, D. E.; Connor, B. J.; Remsberg, R. S. E. E. E.; Tsou, J. J.; Parrish, A. *J. Geophys. Res.* **1995**, *100*, 11 191.
(20) Jucks, K. W.; Johnson, D. G.; Chance, K. V.; Traub, W. A.; Salawitch, R. J.; Stachnik, R. A. *J. Geophys. Res.* **1996**, *101*, 28 785.
(21) Dessler, A. E.; Kawa, S. R.; Considine, D. B.; Waters, J. W. B.; Froidevaux, L.; Kumer, J. B. *Geophys. Res. Lett.* **1996**, *23*, 339.
(22) Slanger, T. G.; Jusinski, L. E.; Black, G.; Gadd, G. E. *Science* **1988**, *241*, 945.
(23) Slanger, T. G. *Science* **1994**, *265*, 1817.
(24) Varandas, A. J. C., to be published.
(25) Price, J. M.; Mack, J. A.; Rogaski, C. A.; Wodtke, A. M. *Chem. Phys.* **1993**, *175*, 83.
(26) Rogaski, C. A.; Price, J. M.; Mack, J. A.; Wodtke, A. M. *Geophys. Res. Lett.* **1993**, *20*, 2885.
(27) Rogaski, C. A.; Mack, J. A.; Wodtke, A. M. *Faraday Discuss. Atmos. Chem.* **1995**, *100*, 229.
(28) Drabbels, M.; Wodtke, A. M. *J. Phys. Chem. A* **1999**, *103*, 7142.
(29) Garrido, J. D.; Caridade, P. J. S. B.; Varandas, A. J. C. *J. Phys. Chem. A* **1999**, *103*, 4815.
(30) Caridade, P. J. S. B.; Zhang, L.; Garrido, J. D.; Varandas, A. J. C. *J. Phys. Chem. A* **2001**, *105*, 4395.
(31) Caridade, P. J. S. B.; Betancourt, M.; Garrido, J. D.; Varandas, A. J. C. *J. Phys. Chem. A* **2001**, *105*, 7435.
(32) Zhang, L.; Varandas, A. J. C. *J. Phys. Chem. A* **2001**, *105*, 10 347.
(33) Balakrishnan, N.; Billing, G. D. *Chem. Phys. Lett.* **1995**, *242*, 68.
(34) Hernández-Lamoneda, R.; Hernández, M. I.; Carmona-Novillo, E.; Campos-Martínez, J.; Echave, J.; Clary, D. C. *Chem. Phys. Lett.* **1997**, *276*, 152.
(35) Campos-Martínez, J.; Carmona-Novillo, E.; Echave, J.; Hernández, M. I.; Hernández-Lamoneda, R.; Palma, J. *Chem. Phys. Lett.* **1998**, *289*, 150.
(36) Campos-Martínez, J.; Carmona-Novillo, E.; Echave, J.; Hernández, M. I.; Hernández-Lamoneda, R.; Palma, J. *Eur. Phys. D* **1998**, *4*, 159.
(37) Balakrishnan, N.; Dalgarno, A.; Billing, G. D. *Chem. Phys. Lett.* **1998**, *288*, 657.
(38) Campos-Martínez, J.; Carmona-Novillo, E.; Echave, J.; Hernández, M. I.; Palma, J. *Mol. Phys.* **2000**, *98*, 1729.
(39) Dodd, J. A.; Lipson, S. J.; Blumberg, W. A. M. *J. Chem. Phys.* **1990**, *92*, 3387.
(40) Dodd, J. A.; Lipson, S. J.; Flanagan, D. J.; Blumberg, W. A. M.; Pearson, J. C.; Green, B. D. *J. Chem. Phys.* **1991**, *94*, 4301.
(41) Rensberger, K. J.; Jeffries, J. B.; Crosley, D. R. *J. Chem. Phys.* **1989**, *90*, 2174.
(42) Sappey, A. D.; Copeland, R. A. *J. Chem. Phys.* **1990**, *93*, 5741.
(43) Dodd, J. A.; Lipson, S. J.; Blumberg, W. A. M. *J. Chem. Phys.* **1991**, *95*, 5752.
(44) Chalamala, B. R.; Copeland, R. A. *J. Chem. Phys.* **1993**, *99*, 5807.
(45) Shalashilin, D. V.; Michtchenko, A. V.; Umanskii, S.; Gershenzon, Y. M. *J. Phys. Chem.* **1995**, *99*, 11627.
(46) Varandas, A. J. C.; Yu, H. G. *Mol. Phys.* **1997**, *91*, 301.
(47) Yu, H. G.; Varandas, A. J. C. *Chem. Phys. Lett.* **2001**, *334*, 173.
(48) Hase, W. L., MERCURY: A general Monte Carlo classical trajectory computer program, QCPE#453. An updated version of this code is VENUS96: W. L. Hase, R. J. Duchovic, X. Hu, A. Komornik, K. F. Lim, D.-H. Lu, G. H. Peslherbe, K. N. Swamy, S. R. van de Linde, A. J. C. Varandas, H. Wang, R. J. Wolf, QCPE Bull 1996, *16*, 43.
(49) Varandas, A. J. C. *Chem. Phys. Lett.* **1994**, *225*, 18.
(50) Varandas, A. J. C. *Chem. Phys.* **1982**, *69*, 295.
(51) Caridade, P. J. S. B.; Sabín, J. A.; Garrido, J. D.; Varandas, A. J. C., to be submitted for publication.
(52) Varandas, A. J. C.; Caridade, P. J. S. B. *Chem. Phys. Lett.* **2001**, *339*, 1.
(53) Capitelli, M., Ed. *Molecular Physics and Hypersonic Flows, NATO ASI Series*; Kluwer: Dordrecht, Vol. 482, 1996.